Slow time evolution of two-time-scale reaction-diffusion systems: The physical origin of nondiffusive transport

Damián E. Strier,* Ariel Chernomoretz,† and Silvina Ponce Dawson‡
Departamento de Física Facultad de Ciencias Exactas y Naturales, UBA Ciudad Universitaria, Pabellón I (1428) Buenos Aires, Argentina

(Received 1 August 2000; revised manuscript received 23 October 2001; published 11 April 2002)

We study, from a mesoscopic point of view, the slow time-scale dynamics of a mixture of chemicals in which there is a chemical reaction that occurs much faster than all other processes, including diffusion. For a simple paradigmatic model reaction, it is possible to find a reduced set of dynamical equations analytically. This procedure, which yields the same mean field equations as the macroscopic approach described by Strier and Dawson [J. Chem. Phys, **112**, 825 (2000)], clarifies the physical origin of some of the terms that appear in the reduced reaction-diffusion equations, such as ''negative density dependent cross diffusion terms,'' whose actual meaning is hard to assess within the macroscopic framework. We also present a two-time-scale reactive lattice gas automaton with which it is possible to check the validity of the analytical results and the conditions under which the reduced description holds. Using this lattice gas we also show how the differential interaction with immobile species can give rise to the formation of stable Turing patterns in a system where all the other chemicals diffuse approximately at the same rate.

DOI: 10.1103/PhysRevE.65.046233 PACS number(s): 05.45.−a, 82.20.−w, 05.65.+b, 02.50.−r

I. INTRODUCTION

During the last decades, self-organization in nonequilibrium systems has attracted the attention of an increasing fraction of the scientific community. Theoretical, experimental, and computational approaches to the study of pattern formation have provided a deeper understanding of the mechanisms of self-organization [1,2]. Among nonequilibrium systems, chemical reactions are paradigmatic. There is a growing interest to unravel the physics underlying its richness of behaviors, which includes: excitability, bistability, oscillations, different types of chemical waves, and the formation of stationary inhomogeneous structures. Fundamental questions concerning reaction-diffusion systems also arise in the biochemical and biological realm [3,4]. The theoretical starting point is usually a set of deterministic equations of motion in the form of partial differential equations for the concentrations of the chemicals. These are the so-called reaction-diffusion equations

$$\frac{\partial S_j}{\partial t} = f_j(S_1, \ldots, S_n) + D_j \nabla^2 S_j, \quad 1 \leqslant j \leqslant n, \tag{1}$$

where $S_j(\vec{r},t)$ is the concentration of the jth species $\mathcal{S}_j$ at time t and position $\vec{r}$, and D_j is its diffusion coefficient ($D_j \geqslant 0$). These equations describe the averaged behavior due to the microscopic processes of reactive and nonreactive collisions. Namely, the (usually nonlinear) terms f_j, in Eq. (1) represent the change in the concentrations due to the chemical reactions (using the law of mass action [5]) and to the feeding and removal of the reactants, while the transport (diffusion) term $D_j \nabla^2 S_j$ is a consequence of the random walk that the particles of each species perform due to the nonreactive collisions with the solvent, which is supposed to be much more abundant than the solute species $\mathcal{S}_j$. Similar equations also arise in other physical contexts in which the various variables and terms have other meanings. One of the aims of the theoretical approach to these problems is to predict what sort of solutions are likely to be reached at long times, starting from a given initial condition. Usually, analytic solutions are out of reach and other approaches are followed to study and classify behaviors [6,7]. It is thus important to develop approximate analytical methods to simplify the systems, and to gain insight into the behavior of the equations.

Part of the interest in reaction-diffusion systems grew out of the seminal work by Turing [3], who pointed out that the interplay between nonlinear reaction kinetics and diffusion processes could produce stable inhomogeneous patterns. In this way he introduced a simple mechanism that could explain the occurrence of spatial patterns in biology (see, e.g., [4]). Although there is no definite proof that this type of mechanism is at work in any real biological system, there are some interesting results in this sense [8,9]. For many years, Turing patterns could not be observed in laboratory experiments, partly because they need the chemicals to diffuse at different rates, and this was hard to achieve in the dilute aqueous systems that the community was focusing on. When Turing patterns were finally observed [10,11], a heuristic explanation was provided of why the various chemicals could diffuse at different rates: it was the interaction with immobile species (namely, the gel where the reaction proceeds and the starch molecules that are used for visualization) that effectively rescaled the diffusion coefficient of one of the species involved in the reaction (iodide in this case) [12]. The idea that diffusion is rescaled by the interaction with other species (*buffers*) is also widespread in biology. For example, the interaction of calcium ions with buffers [13] can explain, under

*Email address: strier@df.uba.ar
†Email address: ariel@df.uba.ar
‡Email address: silvina@df.uba.ar

certain assumptions, the dependence of calcium diffusion on calcium concentration in the cytoplasm [14]. The effect of different sorts of buffers (both mobile and immobile) on calcium diffusion and transport in general is a subject of great current interest, since it is believed that buffers tailor the repertoire of spatiotemporal behaviors that the calcium concentration can display [15–17]. Calcium is a universal second messenger that is used by most cells for signaling purposes [18]. Thus, by the differential interaction with buffers, the calcium concentration can behave in various ways that eventually result in different end responses [18].

The underlying common feature in these two types of problems (Turing patterns in laboratory experiments and calcium dynamics in the presence of buffers) is, on one hand, the existence of at least two very different time scales in the reaction-diffusion system. In fact, the rescaling of the diffusion coefficient of a given species is obtained if the reaction with the immobile buffers occurs much faster than diffusion. The other common feature is the fact that it is the slow time variations that are of interest, while the dynamics of the buffers or of the immobile species in the case of the experimental Turing patterns is not. With these two basic ideas in mind, the aim is then to obtain a reduced description of the slow time dynamics in which at least some of the species have disappeared as dynamical variables (usually buffers or enzymes). We derived this reduction systematically in [19] using a two-time-scale analysis [20]. In order to do this we applied perturbation methods, (developed basically for ordinary differential equations) to a case in which the dynamics is described by partial differential equations. We did this in detail for the case of one reversible fast reaction. None of the previous attempts to handle this type of problem involved a systematic multiple-time-scale reduction. Furthermore, they dealt with the paradigmatic buffering equation [21]

$$\mathcal{A}+\mathcal{B}\underset{k_-}{\overset{k_+}{\rightleftharpoons}}\mathcal{C} \tag{2}$$

in which $\mathcal{A}$ is one of the species of interest (e.g., calcium), $\mathcal{B}$ is the free buffer, and $\mathcal{C}$ is the complex that is formed when $\mathcal{A}$ binds to $\mathcal{B}$. On the other hand, the (mostly) heuristic explanations that appear in [22] or [23] hold if the buffer is immobile and in excess (the concentration of $\mathcal{B}$, B, is much larger than the concentration of $\mathcal{A}$, A). The case of calcium reacting according to Eq. (2) in the presence of any amount of either mobile or immobile buffers was addressed in [13], giving rise to what is now called the *fast buffering approximation*. The analysis of [13] mostly focused on the case in which the only relevant processes were the fast reaction (2) and diffusion.

The main motivation for the work that we describe in this paper arises from the following feature of the reduced evolution equations obtained in [19]: even if we start from a set of reaction-diffusion equations of the form of Eq. (1), the final equations are not always of reaction-diffusion type. Furthermore, they contain terms that involve various combinations of concentration gradients and concentrations (which should be associated with nondiffusive transport terms). Only if the fast reaction involves an immobile species that is in excess, the final equations are of reaction-diffusion type, in which case a clear physical picture can be established (see following section). In all other cases, the physical meaning of the nondiffusive transport terms is hard to assess. In order to obtain a physical picture, in this paper we analyze the reduced description from a more microscopic point of view and determine what sort of thermodynamic force the nondiffusive transport terms represent. To this end, we introduce a two-time-scale reactive lattice gas automaton with which we rederive the reduced (mean-field) equations analytically, starting from a mesoscopic picture, and which we implement numerically for different situations of interest. The result is that the extra terms that appear in the reduced equations are not truly ''transport terms,'' but some kind of ''remnants'' of the fast reaction. The fast reaction correlates the local densities of the chemicals and those terms represent the reaccommodation of these densities to satisfy the correlation condition after it is perturbed due to the diffusive transport of the chemicals. The physical picture also provides a better understanding of the accuracy of the reduced description, which we probe with the numerical simulations. All the analytic calculations are done for the case in which Eq. (2) is the only chemical reaction that occurs in the system. However, the conclusions that we draw can be extended straightforwardly to the more general case of the arbitrary reversible fast reaction that we treated in [19] or to systems in which other (slow) reactions coexist with the fast reaction (2). In order to illustrate the last assertion, we show some numerical simulations of the Schnackenberg model [24] in the presence of an immobile substance that interacts with one of the chemicals according to Eq. (2). Such a system mimics the main features of the laboratory experiments in which Turing patterns are observed (which is a consequence of the differential interaction with an immobile species). In fact, we show that the presence of the immobile species yields Turing structures in a region of parameters where otherwise stable patterns would not be found.

The paper is organized as follows: in Sec. II we review the reduction of a reaction-diffusion system within the macroscopic framework applying it to Eq. (2) and discuss the limiting case in which the final equations are of reaction-diffusion type. In Sec. III the fundamentals of the theory of lattice gases are briefly mentioned (for a complete review see [25] and references therein), and an analytical approximation of the lattice gas theory suitable for two-time-scale systems is described. In Sec. IV we apply these ideas to the reaction (2), and show how the results of Sec. II are reobtained within this framework. In Sec. V we describe various numerical implementations of two-time-scale reactive lattice gas automata and show the results of different simulations. Some of the simulations are done to check the validity of the analytic results. Other simulations are done to study the effect of the fast reaction on the formation of patterns. In particular, we show that the Turing space of the Schnackenberg model is enlarged by the fast interaction of the chemicals with an immobile species. Finally, we discuss the central points in the Conclusions.

II. MACROSCOPIC APPROACH: REACTION-DIFFUSION EQUATIONS

Let us consider a system described by Eqs. (1). Let us assume that there is some reaction that occurs much faster than the rest of the processes, so that we can define the small parameter $\varepsilon \ll 1$ as the ratio between the fast and the slow time scales. Then a perturbative analysis in terms of ε may be done and a reduced description of the slow time dynamics may be obtained. We discussed the general case in [19], and over here we will only quote the results in some particular cases. Let us assume that there are three species $\mathcal{S}_1=\mathcal{A}$, $\mathcal{S}_2=\mathcal{B}$, and $\mathcal{S}_3=\mathcal{C}$, where $\mathcal{A}$, $\mathcal{B}$, and $\mathcal{C}$ react according to Eq. (2), on the fast time scale, i.e., $k_-, k_+ \sim \mathcal{O}(1/\varepsilon)$, while the rest of the parameters are of order one or higher in ε. Let us assume that this is the only reaction in which B and C are involved, and that these species are not removed or fed from outside the region where the reactions take place (the gel in the case of the experiments in which Turing patterns are observed or the cytosol in the case of calcium dynamics). Thus, the reaction-diffusion system (1) that we are dealing with is of the form

$$\frac{\partial A}{\partial t} = -k_+ AB + k_- C + g(A) + D_A \nabla^2 A, \tag{3}$$

$$\frac{\partial B}{\partial t} = -k_+ AB + k_- C + D_B \nabla^2 B, \tag{4}$$

$$\frac{\partial C}{\partial t} = k_+ AB - k_- C + D_C \nabla^2 C, \tag{5}$$

where A, B, and C are the concentrations of the various species, D_A, D_B, and D_C their diffusion coefficients, and the term $g(A)$ represents the slow chemical reactions in which the species $\mathcal{A}$ is involved and the feeding and removal of this species. The boundary conditions will be either no flux or periodic. Although this is a relatively simple system, the calculations we describe here can be easily extended to the case in which there are some additional species that are only involved in slow reactions (such as in the Schnackenberg system that we simulate numerically in Sec. V). On the other hand, calcium dynamics in the presence of one buffer is modeled by this set of equations. Although the case of actual experiments in which Turing patterns are observed is much more complicated than the Schnackenberg model, we think that our study captures the essential features regarding the rescaling of the diffusion coefficients. Following the calculations described in [19] we obtain that, after a short transient (of order ε) the various concentrations approach values that evolve on the slow time scale according to

$$\frac{\partial A}{\partial t} = (1-\Gamma_{BA}) g + (1-\Gamma_{BA}) D_A \nabla^2 A - \Gamma_{AB} D_B \nabla^2 B + (1-\Gamma_{AB}-\Gamma_{BA}) \frac{k_+}{k_-} D_C (B\nabla^2 A + A\nabla^2 B + 2\nabla B \cdot \nabla A), \tag{6}$$

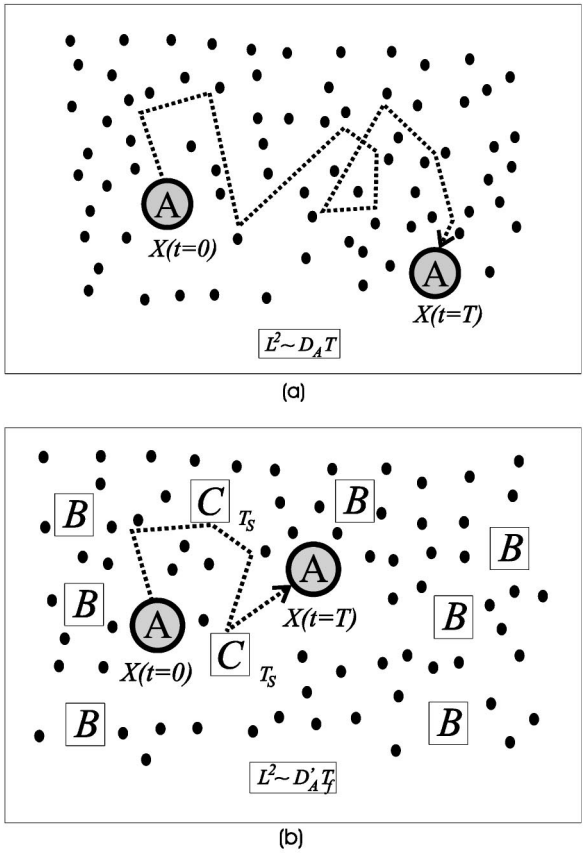

FIG. 1. Random walk of an $\mathcal{A}$ particle in the presence of solvent molecules, drawn as filled circles (a), and in the presence of both solvent and $\mathcal{B}$ particles (b). While in (a) the collisions are nonreactive and the $\mathcal{A}$ particle is free all the time, in (b) it remains bound to each $\mathcal{B}$ particle with which it reacts, to form the complex $\mathcal{C}$ during a time of the order of $1/k_-$.

$$\frac{\partial B}{\partial t} = -\Gamma_{BA} g + (1-\Gamma_{AB}) D_B \nabla^2 B - \Gamma_{BA} D_A \nabla^2 A + (1-\Gamma_{AB} - \Gamma_{BA}) \frac{k_+}{k_-} D_C (B\nabla^2 A + A\nabla^2 B + 2\nabla B \cdot \nabla A), \tag{7}$$

$$C = \frac{k_+}{k_-} AB, \tag{8}$$

where

$$\Gamma_{AB} = \frac{A}{k_d + A + B}, \quad \Gamma_{BA} = \frac{B}{k_d + A + B}, \quad k_d \equiv \frac{k_-}{k_+}, \tag{9}$$

and g is a function of A.

Both in the case in which B and C are immobile and in the case of the dynamics of cytosolic calcium in the presence of buffers, the diffusion coefficients of the free buffer D_B and of the complex D_C are similar. Therefore, we will further assume that $D_C = D_B$. It then follows that, if at $t=0$ it is $B + C = B_T$, with B_T homogeneously distributed in space, then $B + C = B_T$ at all points in space during the whole evolution. This follows clearly from adding Eqs. (4) and (5). Using this

conservation law the system (6)–(8) may be further reduced to one evolution equation for A plus the algebraic equations $B=k_dB_T/(k_d+A)$ and Eq. (8) [26]. Clearly, this final evolution equation is not, in general, of reaction-diffusion type. Furthermore, even in the case in which $D_C=D_B=0$, for which most of the terms vanish, the transport of the $\mathcal{A}$ particles is not exactly diffusive, since the effective diffusion coefficient, $(1-\Gamma_{BA})D_A$, is concentration dependent. There is a limiting case in which the dependence on the concentration can be neglected, namely, when the solution is so dilute that $A \ll k_d$ and $A \ll B_T$. In that case, the effective diffusion coefficient is $(1-\Gamma_{BA})D_A \approx k_d/(k_d+B_T)D_A$. This has a clear microscopic interpretation that we illustrate in Fig. 1.

Figure 1(a) corresponds to the microscopic picture that gives rise to the usual diffusion term. In this case, the $\mathcal{A}$ particles perform a random walk due to the nonreactive collisions with the solvent molecules. Thus, the mean distance L that the particle transverses during a total time T scales as $L^2 \sim TD_A$, with D_A the diffusion coefficient (which is proportional to the mean free path of the $\mathcal{A}$ particles in the presence of the solvent). Figure 1(b) corresponds to the case in which the $\mathcal{A}$ particles also react with an immobile buffer that is in excess, $\mathcal{B}$. Thus, when each $\mathcal{A}$ particle moves in the medium, sometimes it encounters a solvent molecule with which it collides changing its direction instantaneously, and other times it encounters a $\mathcal{B}$ particle and, with a certain probability, reacts and stays bound to it for a time $T_s \approx 1/k_-$. Then, if one looks at one particle during a total time T, only a fraction of this time T_f is used by the particle to move around. Then, the mean distance L, in this case, will scale with the fraction T_f as $L^2 \sim T_f D_A'$, where D_A' is proportional to the mean free path in the presence of both solvent and $\mathcal{B}$ particles. However, if the solvent is much more abundant than $\mathcal{B}$, then we may assume that $D_A' \approx D_A$. Notice that this condition is completely hidden in the macroscopic description. If the concentration B is much bigger than A, then most of the $\mathcal{B}$ particles will be free at any given time so that $B \approx B_T$. This also implies that one can look at each $\mathcal{A}$ particle independently, without having to consider what the other $\mathcal{A}$ particles are doing at any given time. Then we may estimate the number of reactive collisions that one $\mathcal{A}$ particle suffers during the total time T as $k_+B_TT_f$, since it can only react while it is free (i.e., during the fraction T_f). If the particle stays bound during a time $T_s \approx 1/k_-$ after each reaction, then the total time during which it is bound is $k_+B_TT_f/k_-$, and the fraction during which it is free satisfies $T_f = T - k_+B_TT_f/k_-$ from which we get $T_f = k_dT/(k_d+B_T)$. This implies that $L^2 \sim TD_Ak_d/(k_d+B_T)$. Thus, the transport is diffusive with an effective diffusion coefficient that is equal to $D_Ak_d/(k_d+B_T)$. Although this limiting case has a clear microscopic interpretation, the physical meaning of what we could call cross-diffusion terms or of the nondiffusive ones that appear in Eqs. (6) and (7) is not clear at all. In the following sections we try to elucidate the physical meaning of these terms by determining what their microscopic origin is.

III. MESOSCOPIC APPROACH: LATTICE GAS THEORY

Reaction and transport processes can be modeled by means of a reactive lattice gas automaton (RLGA) that captures the essentials of the microscopic reactive molecular dynamic scheme [25,27]. Within this framework, each species is described by the number of particles of each given velocity residing at the sites of a regular lattice. The evolution occurs at discrete time steps, when each particle undergoes a random walk between the lattice sites (diffusion), and reactive collisions occur (when a certain number of particles meet at a lattice site a reaction occurs according to some prescribed probability). Lattice gas methods are clearly faster than full molecular dynamics simulations, because they involve some degree of coarse graining that allows the study of the evolution for long time scales, treating the shorter time scales in a simplified fashion. Most RLGA assume an exclusion principle that restricts the number of particles of each species at a node, with a given velocity. The exclusion principle allows the dynamics to be simulated very efficiently, and also prevents particle density from building up in certain regions of space. On the other hand, it leads to restrictions on both the species densities and the complexity of the reaction schemes to be analyzed. Furthermore, it causes the particles to obey a Fermi-Dirac statistics that is difficult to justify on physical grounds [28]. In this paper we abandon the exclusion principle, and allow for an arbitrary number of particles to reside at each node of the lattice [28–30]. This is not the first time that the exclusion principle is dropped for reactive lattice gas automata. In fact, our numerical implementations of the lattice gas follow Ref. [29] in one case and Ref. [28] in another one.

As mentioned before, lattice gases imply some degree of coarse graining. We assume that each node represents a neighborhood occupied by a large number of particles. Thus, our description cannot describe inhomogeneities that occur at spatial scales that are smaller than the distance between two nodes. Given that we do not use the exclusion principle, keeping track of the particles' velocities becomes unnecessary. Namely, the diffusive transport term is modeled by a random walk in which each step is independent of the previous one (in the sense that the direction in which a particle moves during one step is not correlated to the direction of the preceding step), while the probability that a chemical reaction occurs is velocity independent. Therefore, we will describe the dynamics in terms of the total number of particles of each species at a node and given time, regardless of their velocity. In the Appendix there is a more detailed description of the dynamics in which we show that this point of view is in fact correct. Since we are interested in the derivation of the macroscopic description from the microscopic one, most of the theoretical analysis that we present is done at the level of a lattice Boltzmann scheme, i.e., in terms of averages. Lattice Boltzmann methods are somewhere in the middle between reactive lattice gas automata and finite difference methods [31]. They are suitable whenever one is interested in the evolution of averaged quantities.

A. A two-time-scale lattice gas

The key part of a RLGA is the construction of an evolution operator that gives the state of the lattice (the occupation number at every node) after the reaction and transport (dif-

fusion in our case) operators are applied to the previous state. A useful way to write the evolution operator $\mathcal{E}_s$ for the species s is [38]

$$\mathcal{E}_s = \mathcal{O}^{\pm l_s}(\mathcal{R}\circ\mathcal{T}), \tag{10}$$

where $s \in \hat{S}$, and $\hat{S}$ denotes the set of all the species. The operator $\mathcal{O}$ with a $+l_s$ superscript means l_s applications of the transport operator $\mathcal{T}$ for every reactive operation $\mathcal{R}$, while a $-l_s$ superscript indicates one application of $\mathcal{T}$ every l_s of $\mathcal{R}$. This form of writing the evolution is suitable for numerical purposes, because the desired relations between the diffusion coefficients of different species are easily incorporated in the simulations. As we will show, it is also useful for systems with two different time scales, as the ones we are interested in. In particular, we want to describe the evolution on the slow time scale of systems in which some of the reactions occur on time scales sensitively faster than others and diffusion. In order to simplify the discussion we present here a detailed analysis of the case in which there is only one reaction, which is fast, while diffusion is the only slow process. The results can be easily extended to the case in which there are other slow processes, in particular, slow reactions. To this end we take a relatively large time step τ, half of which we divide in several shorter time steps of size T. The ratio T/τ represents the ratio between the reactive and diffusive time scales. The update of the distribution of particles from time t to time $t+\tau$ consists of one transport step that evolves the distribution from time t to time $t+\tau/2$, followed by l reaction steps ($l \equiv \tau/2T$) that evolve the distribution from $t+\tau/2$ to time $t+\tau$. This splitting is convenient from the analytical point of view. It is reasonable for numerical implementations provided that τ is small enough so that the fraction of particles that move from one site to a neighboring one during the time τ is also small. In fact, we checked the validity of this approximation as we describe in Sec. V. According to this splitting, the reaction operator $\mathcal{R}$ is decomposed as

$$\mathcal{R}^{\tau} = \mathcal{R}^{T}\circ\mathcal{R}^{T}\circ\cdots\circ\mathcal{R}^{T}, \tag{11}$$

where $\mathcal{R}^T$ appears ℓ times and the action of the evolution operator $\mathcal{E}^{\tau} = \mathcal{R}^{\tau}\circ\mathcal{T}^{\tau}$ can be formally written as

$$\mathcal{N}_s(\vec{r}, t+\tau) = \mathcal{E}^{\tau}[\mathcal{N}_s(\vec{r}, t)], \tag{12}$$

where the stochastic variable $\mathcal{N}_s(\vec{r},t)$ is the number of particles of species s that occupy the node of the lattice located at $\vec{r}$, at time t. Since we are interested in the slow time-scale dynamics, we consider the evolution in time steps of size τ. The lattice spacing will be denoted by λ.

For the purpose of deriving the continuous limit from the microscopic dynamics embodied in the explicit form of the evolution operator, two assumptions are usually made. First, it is supposed that the number of molecules of a given species varies smoothly over several lattice spacings. Second, it is assumed that the ensemble average of the product of the occupation number of different species can be broken into the product of the averages of each species separately (usually referred to as the *molecular chaos* hypothesis). While the former hypothesis can be fulfilled in our case, the inefficiency of diffusion for mixing the particles throughout the vessel, and the repeated action of $\mathcal{R}^T$, that rapidly correlates the concentrations of different species at any given node of the lattice, prevents us from applying the latter assumption. In order to obtain a continuous limit, the existence of such correlations poses a hard obstacle. However, if l is large enough another useful approximation can be performed: it may be assumed that the mean concentrations of the various chemicals approximately reach local equilibrium values.[1] These values may be different at different lattice sites, and will depend only on the initial conditions, i.e., the local equilibrium values at each site before the application of the reaction operator. In order to explain why the assumption of local equilibrium may be valid, it is useful to think of the system as composed of a large number of small cells with sides of size λ, centered at each node of the lattice. For the transport of particles between cells to be diffusive over the time scale τ (and effectively modeled by a random walk, as explained later), each particle needs to collide several times with solvent molecules during the time τ. This implies that the mean free path λ_F and the mean frequency ν_C of nonreactive collisions satisfy $\lambda_F \ll \lambda$, $\nu_C \tau \gg 1$. However, λ and τ^{-1} cannot be chosen as small as we wish because there is another constraint: the number of particles inside a cell cannot change too much during the time τ if we want to approximate its time derivative by the ratio between its change and τ. Thus, very few particles must leave the cell during the time τ. This is satisfied if $D\tau/\lambda^2 \ll 1$. This second condition also implies that individual cells can be well approximated as closed systems on the fast time scale (which is much shorter than τ). Therefore, the application of the ''full'' reaction operator $\mathcal{R}^{\tau}$, inside each cell, yields mean values for the various concentrations or, equivalently, mean number of particles $N_s \equiv \langle \mathcal{N}_s \rangle$ that satisfy the equilibrium relationship if $\tau \gg T_{eq}$, with T_{eq} the time it takes for the reaction to equilibrate. The conditions $D\tau/\lambda^2 \ll 1$ and $\tau \gg T_{eq}$ imply that $\lambda \gg \sqrt{DT_{eq}}$. Therefore, the equilibrium condition will be valid provided that the macroscopic quantities do not vary over length scales that are too small. The following diagram shows the evolution from a set of initial conditions $\mathcal{N}_s(\vec{r},0)$ yielding mean values $N_s(\vec{r},t) \equiv \langle \mathcal{N}_s(\vec{r},t) \rangle$:

$$N_s(\vec{r},0) \overset{\mathcal{T}^{\tau}}{\rightarrow} N_s(\vec{r},\tau/2) \overset{\mathcal{R}^{\tau}}{\rightarrow} N_s^{eq}(\vec{r},\tau) \overset{\mathcal{T}^{\tau}}{\rightarrow} N_s(\vec{r},3\tau/2) \overset{\mathcal{R}^{\tau}}{\rightarrow} N_s^{eq}(\vec{r},2\tau) \overset{\mathcal{T}^{\tau}}{\rightarrow} \ldots, \tag{13}$$

where $N_s(\vec{r},n\tau) = N_s^{eq}(\vec{r},n\tau)$ $(n \in \mathbb{N}, n \neq 0)$ are supposed to be equilibrium values,[2] and where we have supposed that both $\mathcal{T}^{\tau}$ and $\mathcal{R}^{\tau}$ advance time by the same amount $\tau/2$. The

[1] Here, the mean concentration corresponds to an ensemble average of $\mathcal{N}_s(x,t)$ over several independent realizations. In Sec. V, this assertion is numerically proved.

[2] We will suppress in the following the superscript denoting equilibrium at times $t = n\tau$ with $n \in \mathbb{N}_+$.

scheme depicted in Eq. (13) emphasizes the fact that, because of the large difference between the times scales over which reactions and diffusion occur, diffusion essentially acts over local equilibrium values that are determined by the relative abundance of the different species before the application of the reaction operator.

As we have already mentioned, we assume that transport is only due to the elastic scattering of particles of the various species, $s \in \hat{S}$, with solvent molecules (i.e., we consider a dilute solution). The following fact is hidden in this kind of description: reactive lattice gas automata treat nonreactive collisions only in a coarse-grained approximation. On the time scales that these lattice gases can resolve, the velocities are not correlated, and each particle can be viewed as performing a random walk. If the medium is supposed to be isotropic, the action of the transport operator $\mathcal{T}^{\tau}$ is to let each particle move to any of its ξ neighboring sites with an equal probability p_s, or to remain stationary with probability $1-\xi p_s$ (no advection is present), where ξ is the number of nearest neighbors ($\xi=2$ in one space dimension and $\xi=4$ for a square lattice in two space dimensions). For simplicity we will consider, in this discussion, a one-dimensional lattice where the coordinate is denoted by x. Higher dimensions can be handled equivalently. We can write the transport operator formally as [29]

$$\mathcal{N}_s(x,t+\tau/2)=\mathcal{T}^{\tau}\mathcal{N}_s(x,t)=\sum_{i=-1}^{i=1}\sum_{\mu=1}^{\infty}\eta^{(i)}_{x+\lambda i,\mu} \times\mathcal{H}(\mathcal{N}_s(x+\lambda i,t)-\mu), \tag{14}$$

where the first sum runs over the components of a random triplet $\vec{\eta}_{x,i}$ taking one of the values (1,0,0), (0,1,0) or (0,0,1) with probabilities p_s, $1-2p_s$ or p_s, respectively, and $\mathcal{H}$ is the Heaviside function defined by $\mathcal{H}(y)=1$ if $y \geqslant 0$, and $\mathcal{H}(y)=0$ otherwise.

The macroscopic description is obtained by taking an ensemble average of $\mathcal{N}_s(x,t)$ over several independent realizations of the system. In practice, however, this average is assumed to be equivalent to some coarse graining or time average [28]. The action of the transport operator (14) on the mean occupation number reduces to moving a constant fraction of particles p_s (generally different for each species) to each neighboring cell. Using Eq. (14), the evolution for the mean numbers can be written as

$$N_s(x,t+\tau/2)=N_s(x,t)+p_s[N_s(x+\lambda,t)+N_s(x-\lambda,t)-2N_s(x,t)]. \tag{15}$$

Using the conservation laws and the relations among the (mean) densities at equilibrium, it is possible to write down the values of $N_s(x,n\tau)$ at each node of the lattice as a function of its initial values $N_s(x,n\tau-\tau/2)$ (before the application of $\mathcal{T}^{\tau}$). Then, a closed system is finally obtained in the form of a coupled set of master equations. Note that this procedure makes it evident that the explicit form of the reaction operator $\mathcal{R}^{T}$ is not important. In fact, any sensible reaction rule must project the local concentration to equilibrium values on the slow time scale.

IV. APPLICATION TO THE CASE $\mathcal{A}+\mathcal{B}\leftrightharpoons\mathcal{C}$

In this section we apply the ideas described in the preceding section to study the reaction (2). To this end, we first note that as there is no feeding or removal of chemicals, the whole system is closed. Thus some quantities are conserved during the reactions [32]. The sum of $\mathcal{A}$ (or $\mathcal{B}$) and $\mathcal{C}$ molecules over all the nodes of the lattice is clearly conserved, because the creation of one type implies the annihilation of the other. Another conservation law arises because each reaction leaves the difference between the total number of $\mathcal{A}$ and $\mathcal{B}$ molecules unchanged. But these conservation laws are global, and do not apply to each cell separately, because diffusion can add or subtract particles at each node independently of reactions. Instead, the following local relations should hold:

$$N_A(x,t+\tau/2)-N_B(x,t+\tau/2)=N_A(x,t+\tau)-N_B(x,t+\tau), \tag{16}$$

$$N_A(x,t+\tau/2)+N_C(x,t+\tau/2)=N_A(x,t+\tau)+N_C(x,t+\tau), \tag{17}$$

$$N_B(x,t+\tau/2)+N_C(x,t+\tau/2)=N_B(x,t+\tau)+N_C(x,t+\tau), \tag{18}$$

where $t=n\tau$. Note that Eqs. (16)–(18) are not all independent. These equations reflect that, during the successive application of the reaction operator on the fast time scale, each cell behaves as a closed system. The equilibrium concentrations—those reached after every application of the projector $\mathcal{R}^{\tau}$—satisfy the algebraic relation

$$A(x,t+\tau)B(x,t+\tau)=k_d C(x,t+\tau), \tag{19}$$

where

$$A(x,t)=N_A(x,t)/\lambda, \quad B(x,t)=N_B(x,t)/\lambda, \quad C(x,t)=N_C(x,t)/\lambda. \tag{20}$$

These equations can be used to obtain the equilibrium values of the local numbers of molecules, as a function of the initial values. Solving Eqs. (16), (17), and (19), the non-negative roots are

$$N_A(x,t+\tau)=\frac{1}{2}[N_A(x,t+\tau/2)-N_B(x,t+\tau/2)-\overline{k_d}+h(x,t+\tau/2)], \tag{21}$$

$$N_B(x,t+\tau)=\frac{1}{2}[N_B(x,t+\tau/2)-N_A(x,t+\tau/2)-\overline{k_d}+h(x,t+\tau/2)], \tag{22}$$

$$N_C(x,t+\tau)=\frac{1}{2}[N_A(x,t+\tau/2)+N_B(x,t+\tau/2) + 2\,N_C(x,t+\tau/2)+\overline{k_d}-h(x,t+\tau/2)], \tag{23}$$

where

$$h(x,t)=[(\overline{k_d}-N_A+N_B)^2+4\overline{k_d}(N_A+N_C)]^{1/2}, \tag{24}$$

and $\overline{k_d}=k_d\lambda$.

From Eqs. (15) and (16), it is straightforward to show that

$$\Delta N_A-\Delta N_B=p_A\mathcal{D}_A-p_B\mathcal{D}_B, \tag{25}$$

where we have introduced the notation

$$\Delta N_s\equiv N_s(x,t+\tau)-N_s(x,t), \tag{26}$$

$$\mathcal{D}_s\equiv N_s(x+\lambda,t)+N_s(x-\lambda,t)-2N_s(x,t).$$

Equation (25) emphasizes that the only source of difference in the relative number of $\mathcal{A}$ and $\mathcal{B}$ particles in any lattice site during the time step τ, is due to the action of the transport operator over each species.

For simplicity we first set $p_C=0$ (i.e., C does not diffuse). Then using Eq. (15) and Eq. (17) we find

$$\Delta N_A+\Delta N_C=p_A\mathcal{D}_A. \tag{27}$$

Because the differences ΔN_s are evaluated at equilibrium by construction, we can make use of Eq. (19). Then

$$\overline{k_d}\Delta N_C=N_A\Delta N_B+N_B\Delta N_A+\Delta N_A\Delta N_B\simeq N_A\Delta N_B + N_B\Delta N_A. \tag{28}$$

Now, we can solve for the variation of N_A as

$$\Delta N_A\left[1+\frac{1}{\overline{k_d}}(N_A+N_B)\right]=p_A\mathcal{D}_A-\frac{N_A}{\overline{k_d}}(p_B\mathcal{D}_B-p_A\mathcal{D}_A). \tag{29}$$

Proceeding in the same way we find

$$\Delta N_B\left[1+\frac{1}{\overline{k_d}}(N_A+N_B)\right]=p_B\mathcal{D}_B-\frac{N_B}{\overline{k_d}}(p_A\mathcal{D}_A-p_B\mathcal{D}_B). \tag{30}$$

Equation (29) [which is completely analogous to Eq. (30)] isolates two components responsible for the time variation of N_A at a given point x. One of them simply accounts for the transport of particles towards and from x. The other one is the most interesting. It indicates that N_A and N_B can also change due to the chemical reaction: when the chemical equilibrium is disrupted by the arrival or departure of $\mathcal{A}$ or $\mathcal{B}$ particles during the diffusive step, the (fast) chemical reaction establishes a new equilibrium and this is reflected in these other terms. Also, if the arrival of $\mathcal{A}$ and $\mathcal{B}$ particles is perfectly balanced, the chances for reacting do not change and then this term would not induce a time variation of N_A. Furthermore, if the number of $\mathcal{A}$ particles is large and/or the probability of having a reactive collision increases, this effect becomes stronger. The derivation also makes clear the key role played by the correlations introduced among the concentrations on the fast time scale [Eq. (19)]. This equation underlies both, the above reasoning and the prefactor that multiplies the time variations of N_A (and N_B).

The final step is to find the continuum limit of these equations. The usual way to do this is to let $\tau\to 0$ and $\lambda\to 0$, with the ratio λ^2/τ finite. Writing the concentrations as in Eq. (20), multiplying Eqs. (29) and (30) by $1/\tau$, defining $D_A=p_A\lambda^2/\tau$ and $D_B=p_B\lambda^2/\tau$, and taking the above-mentioned limit, we obtain Eqs. (6) and (7) with $D_C=0$. Now we see that behind the diffusionlike appearance of some of the terms in these equations, (e.g., the self-diffusion and the cross-diffusive terms), there is a common chemical origin. The fact that they can be expressed in the form of a Laplacian is because the differences in the concentrations of neighboring sites regulate the rate of the reactions.

In the case where $D_C\neq 0$ (i.e., $p_C\neq 0$), the same reasoning leads us to the equations

$$\Delta N_A-\Delta N_B=p_A\mathcal{D}_A-p_B\mathcal{D}_B, \tag{31}$$

$$\Delta N_A+\Delta N_C=p_A\mathcal{D}_A-p_C\mathcal{D}_C,$$

$$\Delta N_B+\Delta N_C=p_B\mathcal{D}_B-p_C\mathcal{D}_C,$$

from which we get Eqs. (6)–(8) in the continuous limit.

V. NUMERICAL IMPLEMENTATION OF THE TWO-TIME-SCALE LATTICE GASES

In this section we describe the numerical implementation of two (closely related) types of reactive lattice gas automata, that follow the ideas described in the previous sections. In all cases the evolution operator $\mathcal{E}$ (i.e., the combination of the reaction and transport operators) acts on a regular lattice of size L (linear or square) with periodic boundary conditions. As mentioned before, we do not impose the exclusion principle in any of these versions.

We also present some numerical simulations that we performed with these lattice gases. First, a situation in which there are three species, $\mathcal{A}$, $\mathcal{B}$, and $\mathcal{C}$ in a closed vessel that react on the fast time scale according to Eq. (2) and diffuse on the slow time scale. Initially, $\mathcal{B}$ and $\mathcal{C}$ are homogeneously distributed and there is a local accumulation of $\mathcal{A}$ particles that starts to spread within the system. In this case the nonlinear rescaling of the diffusion coefficients is only a transient effect because the system is unable to support inhomogeneous structures, so the density-dependent diffusion coefficients approach constant values. In spite of this, the simulations are good to check the validity of (i) the slow-time-scale reduction of the evolution equations, testing its limits of applicability, (ii) the physical interpretation that we provided of the microscopic origin of the various transport terms.

The second situation that we have simulated is one that may support stationary inhomogeneous structures. Namely,

we have simulated an open system with six species, $\mathcal{A}$, $\mathcal{S}_2$, $\mathcal{X}$, $\mathcal{Y}$, $\mathcal{B}$, and $\mathcal{C}$, that react according to the scheme

$$\mathcal{A} \underset{k_{-1}}{\overset{k_{+1}}{\rightleftharpoons}} \mathcal{X}, \quad \mathcal{Y} \overset{k_2}{\rightarrow} \mathcal{S}_2, \quad 2\mathcal{A}+\mathcal{S}_2 \overset{k_3}{\rightarrow} 3\mathcal{A},$$

$$\mathcal{A}+\mathcal{B} \underset{k_{-4}}{\overset{k_{+4}}{\rightleftharpoons}} \mathcal{C}. \tag{32}$$

The set of the first three reactions in Eq. (32) constitute the so-called Schnackenberg model [24]. By keeping the concentration of $\mathcal{X}$ and $\mathcal{Y}$ at certain nonequilibrium values, it is possible for this system to display homogeneous periodic oscillations in the concentrations of $\mathcal{A}$ and $\mathcal{S}_2$. Furthermore, if the ratio between the diffusion coefficients $d=D_S/D_A$ is greater than a certain threshold, stationary inhomogeneous structures can also be formed [4]. An important motivation for studying this system is that it is believed that a similar mechanism controls some features of the unicellular alga *Acetabularia*. The experimental evidence suggests that the relevant species involved in the appearance of a Turing structure in this organism are calcium ions ($\mathcal{A}=Ca^{2+}$) and cyclic-AMP ($\mathcal{S}_2=$cAMP) [4,33]. Nevertheless, there is a problem in proposing this simple model as an explanation of the observations: the ratio between the (free) diffusion coefficients of Ca^{2+} and cAMP is below the threshold value of the Turing instability. However, Ca^{2+} is strongly buffered *in vivo*. Then, it is possible that its diffusion coefficient is effectively rescaled by its interaction with buffers in such a way that the ratio of effective diffusivities and the rescaled reaction kinetics allow for the formation of stable patterns. With this in mind, we added the fourth equation to account for the interaction of Ca^{2+} with an immobile buffer $\mathcal{B}$. As in Eq. (2), we assume that the binding and unbinding of $\mathcal{A}$ with $\mathcal{B}$, occurs on a shorter time scale than any other process in the system.[3]

The aim of this second set of simulations is twofold. First, we want to show that the conclusions obtained in Sec. III can also be applied to other (more complex) situations. Second, we want to show a simulation that mimics the main features of the laboratory experiments in which Turing patterns are observed. Namely, that the differential interaction with an immobile species can enlarge the region of parameter space for which stable Turing patterns exist.

A. The algorithms

We include here a brief description of the algorithms. In the first case [the only reaction is Eq. (2) and occur on a fast time scale compared to the slow diffusion process] the updating process is split up in two. Namely, during half of the time step, the ''one-step'' reaction operator associated with the fast reaction, $\mathcal{R}_{\mathcal{F}}^{T}$, is applied l times ($l\sim\tau/T$), each time to a new set of particles that are randomly chosen inside each cell. Whether the reaction actually occurs after each application of $\mathcal{R}_{\mathcal{F}}^{T}$ or not is also decided randomly, with a certain probability. During the other half, the transport operator $\mathcal{T}^{\tau}$ is applied to one set of randomly chosen particles. We implemented two versions of how to do this splitting, which differ by how the ratio between the number of times that each operator is applied, l, is chosen: while in one version l is fixed, in the other one it is chosen randomly among a set of values with fixed mean value l. We compared both approaches finding a very good agreement between them. Most of the simulations that we show correspond to the version with fixed l. The transport operator ($\mathcal{T}$) moves each particle of species s to any of its adjacent lattice points with probability p_s or leaves it fixed with probability $1-4p_s$. In all the simulations, we assumed that the probability p_s was greater for $\mathcal{A}$ than for $\mathcal{B}$ and $\mathcal{C}$. This means that the free diffusion coefficient of $\mathcal{A}$ is larger than those of $\mathcal{B}$ and $\mathcal{C}$. Regarding the reactions, we basically followed Ref. [29]. The scheme works like this: if there are $\mathcal{N}_A$ and $\mathcal{N}_B$ particles at a site, the reaction operator removes one $\mathcal{A}$ particle and one $\mathcal{B}$ particle and adds one $\mathcal{C}$ particle at that site, with probability $P_{AB}\mathcal{N}_A\mathcal{N}_B$. Conversely, if there are $\mathcal{N}_C$ particles, one of them is replaced by an $\mathcal{A}$ and a $\mathcal{B}$ particle with probability $P_C\mathcal{N}_C$. The short time step T is chosen so as to keep both $P_{AB}\mathcal{N}_A\mathcal{N}_B$ and $P_C\mathcal{N}_C$ below unity for all times at any of the lattice points. The proper link between the rate constants and the probabilities for a given reaction to occur, follows the one described in [29]. That is, k_+ is associated with the ratio P_{AB}/T and k_- to P_C/T. In all the simulations we used $k_d=k_-/k_+=1$ for the fast reaction.

For the scheme (32) some minor changes were introduced. The transport operator works similarly as the one described for the previous scheme. Regarding the reactions, we basically followed Ref. [28]. For example, in the reaction

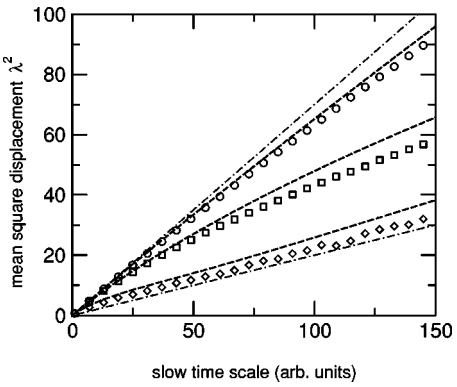

FIG. 2. Net mean-square displacement of $\mathcal{A}$ particles as a function of time measured on the slow time scale in a square lattice with $L=50$. Circles correspond to ($N_A=75\,000$, $N_B=N_C=5000$), squares to ($N_A=N_B=N_C=75\,000$), and diamonds to ($N_A=5000$, $N_B=N_C=75\,000$). For the three cases a δ-like initial condition for $\mathcal{A}$ was used, while $\mathcal{B}$ and $\mathcal{C}$ were randomly distributed. The straight dash-dotted lines correspond to the case of pure diffusion with $p_A=0.7$ (steeper slope) and $p_A=0.2$. The long-dashed lines correspond to the mean-square displacement obtained with simulations of the reduced set of Eqs. (6)–(8) for equivalent parameter values and initial conditions (see text).

[3]This assumption seems to be reasonable for various endogenous calcium-immobile buffers, such as troponin-C [34].

$\mathcal{A}\rightarrow\mathcal{X}$, a random number is picked for each $\mathcal{A}$ particle to decide, according to a certain probability (which we call $P_{\mathcal{A}\rightarrow\mathcal{X}}$), if it transforms into an $\mathcal{X}$ particle or not. For the trimolecular reaction, the situation is a little bit more complicated: all possible triplets of two $\mathcal{A}$ particles and one $\mathcal{S}_2$ particle are listed and a random number is picked sequentially to decide, with a certain probability ($P_{\mathcal{S}\rightarrow\mathcal{A}}$), if each triplet transforms into three $\mathcal{A}$ particles or not. If it does, then all the triplets that contained the two $\mathcal{X}$ particles that reacted are removed from the list. The sequence stops when a random number has already been picked for all the triplets. It is a simple mathematical exercise to show that this procedure yields the law of mass action when the limit of a large number of particles is taken.

B. Numerical simulations

We discuss first the results for the case of three species that react fast according to Eq. (2) and diffuse slowly. Figure 2 shows the time evolution on the slow time scale of the net mean-square displacement of the particles of species $\mathcal{A}$, i.e., $\langle[\vec{r}(t)-\vec{r}(0)]^2\rangle$ where the average runs over all $\mathcal{A}$ particles (its initial number being equal to $\mathsf{N_A}$). The species $\mathcal{B}$ and $\mathcal{C}$ were initially randomly distributed over all lattice sites, while the $\mathcal{A}$ molecules were concentrated on a 3×3 spot located at the center of a rectangular lattice of size $L=50$. In all the simulations, the free diffusion coefficient of $\mathcal{A}$ was 3.5 times greater than that corresponding to $\mathcal{B}$ and $\mathcal{C}$ ($p_A=0.7/4$, $p_B=p_C=0.2/4$). The curves correspond to simulations with different values of the relative initial number of particles ($\mathsf{N_A}$, $\mathsf{N_B}$, and $\mathsf{N_C}$). The value of l was fixed at 10^4 for all the simulations. We included as references two dash-dotted lines that correspond to the case of pure diffusion with $p_A=0.7$ (the one with the steeper slope) and $p_A=0.2$. We found that, when the total amount of $\mathcal{A}$ particles released is in large excess with respect to $\mathcal{B}$, the behavior is practically diffusive (linear), with diffusion constant very close to the free diffusion coefficient (the curve with the empty circles in Fig. 2). This is intuitively clear, because the overwhelming majority of $\mathcal{A}$ particles are not bound forming $\mathcal{C}$. Thus, they diffuse at their normal rate, since the reaction effectively operates over a small fraction of particles. The rest of the particles move at their normal rate. When the amount of $\mathcal{B}$ particles is increased, the plot of the net mean square displacement ceases to be a straight line, indicating that the transport is not purely diffusional (the empty square curve). In this situation, it becomes apparent from the figure that the effect of the reaction cannot be understood as a simple rescaling of the free diffusion coefficient by a constant factor. Instead, a time dependence of the diffusion coefficient arises, that follows from both, the nonlinear density dependence of the ''diffusion coefficients,'' and the particular δ-like initial condition chosen for $\mathcal{A}$. At short times, however, even when the density of $\mathcal{A}$ in the whole lattice might be comparable to that of $\mathcal{B}$, in the small region where the $\mathcal{A}$ particles are concentrated, a situation similar to the first case occurs. So, no major departures from the linear behavior are expected (the initial slope is approximately 0.7). However, as time evolves, the particles that penetrate inside the region where the density of $\mathcal{A}$ is small, have a high probability of reacting, and consequently its effective mobility slows down. As the inhomogeneity disappears (which is the ultimate fate for this particular system), the diffusion coefficients approach stationary values that depend only on the initial densities, and the dissociation rate. The curve with diamonds shows the case when $\mathcal{B}$ is in excess with respect to $\mathcal{A}$. The behavior is again almost diffusive, and the measured diffusion coefficient corresponds to the slow diffusion of the $\mathcal{C}$ particles, i.e., $p_A=0.2$ (at early times the slope is higher for the same reason as explained before).

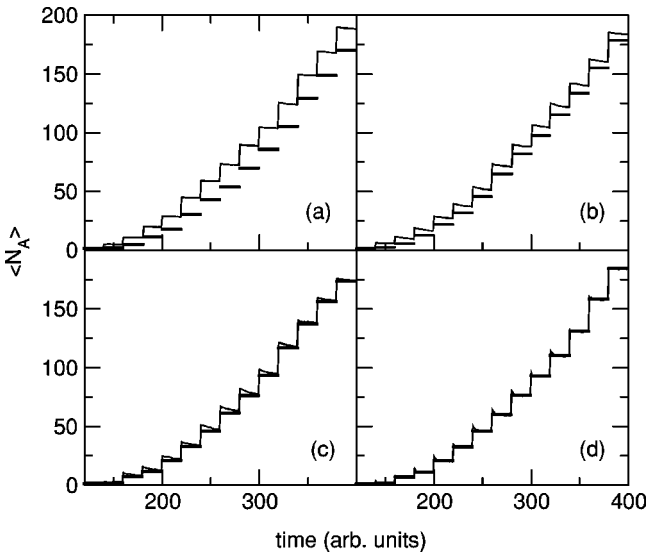

FIG. 3. Evolution on the fast time scale of N_A and N_A^{eq} averaged over a 3×3 neighborhood around the exploratory point, located ten lattice sites apart from the center. The same initial distribution as in Fig. 2 was used with $\mathsf{N_A}=250\,000$, $\mathsf{N_B}=\mathsf{N_C}=100\,000$. The thicker curves correspond to the local equilibrium values of N_A and the thinner ones to the actual number of $\mathcal{A}$ particles. We used $l=10^3$, $l=10^4$, $l=5\times10^4$, and $l=3\times10^5$ in (a), (b), (c), and (d), respectively.

In order to contrast these results against the ''effective diffusion coefficient'' that the macroscopic reduced description yields, we also show in Fig. 2 curves of $\langle r^2\rangle(t)\equiv\int_0^R r^2[A(r,t)-A^*(r,0)]rdr/\int_0^R[A(r,t)-A^*(r,0)]rdr$ vs t, with $A(r,t)$ a solution of the reduced set of macroscopic equations [Eq. (6) with $D_B=D_C$ plus the algebraic relations $B=k_dB_T/(k_d+A)$ and $C=AB_T/(k_d+A)$, in this case] with initial condition $A(r,0)=A^*(r,0)+\mathsf{N_A}\delta(r)$ in a circular domain of radius $R=25$, with boundary condition $\partial A/\partial r=0$ at $r=R$. Notice that the initial conditions used for the lattice gas simulations do not satisfy the local equilibrium conditions that are implicit in the reduced macroscopic equations. As mentioned in [19], the initial condition for the reduced set of equations, at each point in space, is equal to the asymptotic (equilibrium) solution that the actual initial concentrations would approach if the fast reaction were the only process (and there was no spatial coupling). Given that the initial condition of the lattice gas, away from the small 3×3 spot where all $\mathcal{A}$ particles are located, corresponds to uniform initial concentrations given by $[A]_0=0$, $[B]_0$

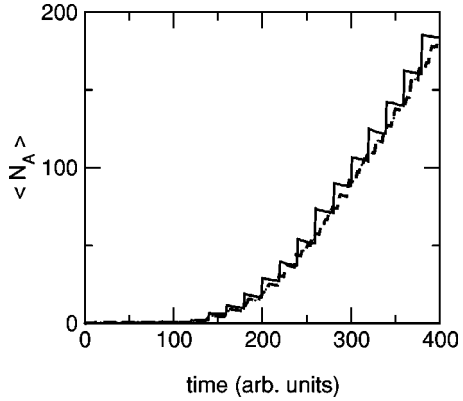

FIG. 4. Similar to Fig. 3, but for a lattice gas with a variable number of diffusion to reaction time steps. The solid lines correspond to one realization, while the dashed line is the average over 80 such realizations.

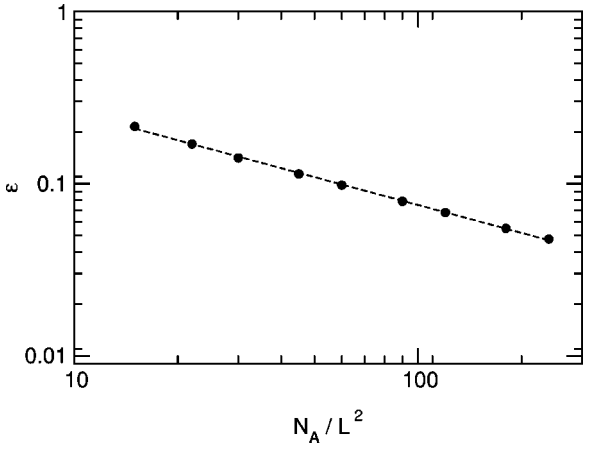

FIG. 6. Relative error between the prediction of Eq. (6) and the values obtained in the simulations as a function of the total number of $\mathcal{A}$ particles present in the lattice.

$=N_B/L^2$, and $[C]_0=N_C/L^2$, then the initial condition of the reduced set of equations away from the small spot is the spatially homogeneous equilibrium value $A^*(r,0)$ that satisfies $kA^*(r,0)B^*(r,0)=k'C^*(r,0)$, $B^*(r,0)+C^*(r,0)=[B]_0+[C]_0$, and $A^*(r,0)+C^*(r,0)=[C]_0$. The value of $A^*(r,0)$ is not equal to zero for any of the simulations. Thus, the calculation of $\langle r^2\rangle$ obtained from the simulations of the reduced set of equations as defined before corresponds to an average of the mean-square displacement over those $\mathcal{A}$ particles that are injected in the small spot, not over all $\mathcal{A}$ particles, as it is the case for the lattice gas simulations. This is the explanation of why the values of mean-square displacement obtained from the reduced set of equations are larger than those obtained with the lattice gas. Namely, initially the injected $\mathcal{A}$ particles diffuse, on average, at their free diffusion rate, while those that come from a chemical decay of the $\mathcal{C}$ particles [those that are included in $A^*(r,0)$] diffuse at a rescaled diffusion rate that is smaller. Thus, taking the average over all particles reduces the mean-square displacement when compared with the average over the injected particles. In any case, we observe that the slope of the curves eventually approach similar values for both sets of simulations. We then conclude that the effective diffusion coefficients of the reduced set of equations provide an accurate estimate of how the particles spread, given that the separation of time scales is sufficiently large.

Figure 3 shows the evolution of N_A and N_A^{eq} as a function of time, measured on the fast time scale, at a fixed (exploratory) point located ten lattice points away from the center, where a δ-like initial condition was again set for N_A. The other species were randomly distributed. The plots correspond to different values of l. For large l [Fig. 3(d), $l=3\times10^5$ and Fig. 3(c), $l=5\times10^4$], the reaction rapidly drives the system towards the equilibrium values, and thus, as expected from Eq. (13), diffusion essentially acts over the local equilibrium values determined by the relative abundance of

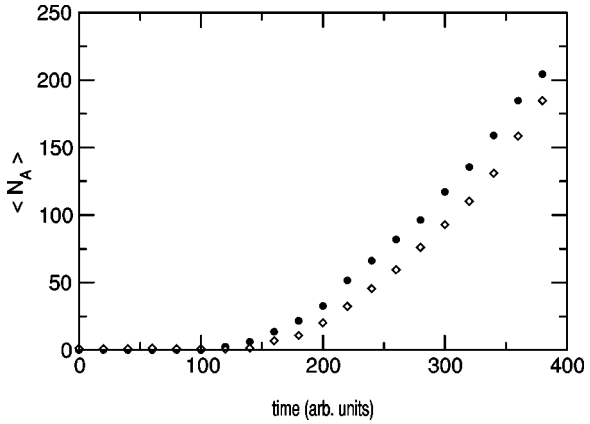

FIG. 5. Evolution of $N_A(\bar{x},t)$ averaged around the exploratory point, $\bar{x}$, as described in Fig. 3, after the chemical reaction takes place for $l=10^2$ (filled circles) and $l=3\times10^5$ (empty diamonds).

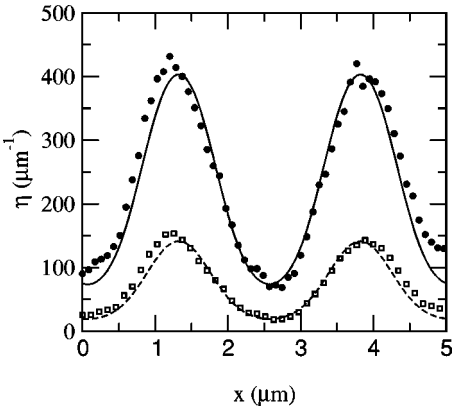

FIG. 7. Turing pattern obtained from the modified version of the Schnackenberg model at long times, with a diffusion ratio $d=4$ below the standard critical value. The y axis corresponds to $\eta_s \equiv \mathcal{N}_s/\lambda$, averaged over 2.5×10^5 successive states of the lattice gas. Solid circles (empty squares) correspond to $\mathcal{C}$ ($\mathcal{A}$) particles. The solid line is the steady-state solution numerically found by integration of the set of reaction difusion equations, for the concentration of $\mathcal{C}$ molecules, while the dashed line stand for expected the concentration of $\mathcal{A}$ (see the text for more details).

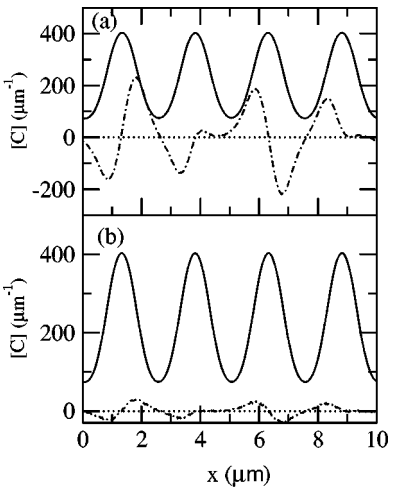

FIG. 8. Concentration profile of $\mathcal{C}$ (solid line) and difference between this concentration and the one obtained from Eq. (19) multiplied by 10^6 (dashed line) at times $t=0.03$ s (a) and $t=0.038$ s (b).

the different species. It is in this circumstance that the continuum equations (6) and (7) hold. When l is decreased, the system is unable to reach the local equilibrium values. This is shown in Fig. 3 where the divergence between the actual and the equilibrium paths is manifest [Fig. 3(b), $l=10^4$ and Fig. 3(a), $l=10^3$]. Because of the initial condition, the actual number of particles that reach the exploratory point is above the equilibrium values. Again, given that the system eventually approaches a homogeneous state, the departure of the two curves is only transient.

In Fig. 4 we plot the same evolution as that of Fig. 3(b), but in this case, the ratio between the number of times that the diffusion and the reaction operators are applied is picked up randomly. This rule, which makes more sense physically, yields the desired ratio between time scales only on average. The solid lines correspond to one realization, while the dashed line is the average over 80 independent realizations. As expected, the artificially rippled form of each individual realization gets smoother when the ensemble average is taken. In this way, the local approach to equilibrium, which seems rather artificial in Fig. 3 or in the individual realization of Fig. 4, is somehow ''hidden'' in the averaged solution. It is this averaged solution that has to be contrasted against the solution of the partial differential equation.

In Fig. 5 we plot the value of N_A, at the same exploratory point, as a function of time, before the application of the diffusion operator for $l=10^2$ and $l=3\times10^5$. The initial condition is the same as before. As a result of the different effective diffusion coefficients, the times at which the front passes through the point are shifted. At any given time, the amount of unbound $\mathcal{A}$ particles is larger for lower l values. Thus, as we can see from the examples of Fig. 2, the effective diffusivity is larger and the front arrives earlier for the case depicted with filled circles ($l=10^2$) than for the one with empty diamonds ($l=3\times10^5$).

Figure 6 shows the relative error between the predicted value for the occupation number, $N_A(\vec{r},t+\tau)$, that follows from Eq. (6), and the actual value that follows from the simulation, averaged over the whole lattice. In this case, the particles were randomly distributed initially, and p_C was set to zero. As expected (see [32]) the error decays as the square root of the number of particles.

We now discuss the results obtained for the case of six chemical species reacting according to the scheme (32). In Fig. 7, we show the results of a simulation in one dimension. Initially, all of the particles were randomly located at the nodes of a lattice with periodic boundary conditions (similar results were obtained using zero flux boundary conditions). We divided the lattice of total length $L=10$ μm into 350 cells, and the evolution took place with a time step of 2×10^{-7}s. The diffusion coefficients of $\mathcal{A}$ and $\mathcal{S}_2$ were $D_A=40$ μm^2/s and $D_{S_2}=160$ μm^2/s. We initially set $\mathsf{N_A}=700$, $\mathsf{N_{S_2}}=3100$, $\mathsf{N_X}=780$, $\mathsf{N_Y}=630$, $\mathsf{N_B}=12\,000$, and $\mathsf{N_C}=2000$. The microscopic reaction probabilities per unit time were $P_{A\to X}=0.0002$, $P_{X\to A}=0.000\,02$, $P_{Y\to S_2}=0.0002$, $P_{S_2\to A}=0.000\,02$, $P_{B\to C}=0.02$, and $P_{C\to B}=0.2$ measured in s^{-1}. As mentioned before, if the fast reaction with the buffer were not included, this system would not support stable Turing patterns for any set of reaction rates (or here, reaction probabilities), because the diffusion ratio, $d\equiv D_{S_2}/D_A=4$, is below the critical value, $d_c\sim6$ (see [4]). However, because of the interaction with the (immobile) buffer $\mathcal{B}$, a Turing pattern spontaneously emerges from the uniform initial condition, as we show in Fig. 7. This figure corresponds to a time average of the occupation numbers (divided by λ) of $\mathcal{A}$ and $\mathcal{C}$ particles over a time interval of length 0.05 s, taken after the first 0.5 s of the evolution have elapsed. While the successive microscopic states change permanently, after a transient time, fluctuations on the occupation number occur around a well-defined average as the one displayed in this figure. Given that the correlations between successive states rapidly dissapear, the time average is equivalent to an ensemble average over many independent realizations, and thus, the behavior observed in Fig. 7 is expected to be found at the macroscopic level. We indeed checked this assertion by comparing the result of the lattice gas with the numerical integration of the macroscopic laws of motion, i.e., the set of four reaction diffusion equations governing Eq. (32) (similar results were obtained integrating the system after the rescaling procedure was performed, as described in [19]). The solid and dashed lines in Fig. 7 correspond to the time-independent concentration profile of $\mathcal{A}$ and $\mathcal{C}$ species, respectively. It can be seen that there is a very good agreement between the results of these two independent approaches.

Finally we check if the concentrations satisfy the local equilibrium condition [Eq. (19) with $k_d=k_{-4}/k_4$] in this case. As mentioned before, this is a consequence of the time-scale separation and it is the main assumption underlying the fast buffering approximation or the reduced description of [19]. It is important to note that when the stationary state has been reached the equilibrium condition must be satisfied. However, local departures may occur during the evolution, especially in those regions with large concentration gradients, where diffusion is not that slow compared to the fast

reaction. We show in Fig. 8 the concentration profile of $\mathcal{C}$ (solid line) at long times ($t=0.03$ s), when the concentration is close to the stationary pattern, and the difference between this concentration and the one obtained from Eq. (19), at two different times. The dashed line corresponds to time $t=0.03$ s and the dotted line to $t=0.038$ s. There we observe that the fast buffering approximation is a reliable assumption in this case. We also observe that the error of this approximation gets smaller for larger times and never exceeds 10^{-4}.

VI. CONCLUSIONS

In most experimental situations, the behavior of a chemical or biochemical system can only be observed on time scales that are large compared with the times required for many of the reactions to reach equilibrium. The evolution is then governed by a reduced set of equations that describe the collapsed spatiotemporal dynamics onto a lower-dimensional manifold. Along with this spontaneous collapse, sometimes exogenous chemicals that are added to the systems for different purposes, can further reduce the degrees of freedom. The exogenous particles can alter dramatically the reaction kinetics and the rate of diffusion of the molecules involved. Perhaps the most striking evidence of this assertion is the role played by starch molecules loaded in gels of continuously fed reactors in the CIMA reaction, where Turing structures were first observed [10,11]. Initially, starch was loaded for visualization purposes, but the evidence suggests that the selective interactions of the iodide molecules with the starch provides the necessary difference between the diffusion coefficients of iodide and chlorite for Turing patterns to appear [12,22]. Another example refers to the existence of Turing structures from biochemical mechanisms at work in cells. It is well known that the mechanism that controls the hair spacing in the whorl of the unicellular alga *Acetabularia* can be modeled using the Schnackenberg reaction diffusion equations, identifying the morphogens with calcium ions and cyclic-AMP [4,33]. While the experiments suggest that the use of this simple model is well grounded, the relation between the diffusivities needed for the emergence of a Turing instability does not hold in reality. Taking into account that Ca^{2+} is strongly buffered *in vivo*, it is still possible that the rescaling introduced by a fast reaction with a buffer allows for the appearance of patterns with a realistic ratio of diffusivities. In this regard, the modified version of the Schnackenberg reaction diffusion system analyzed in this paper, shows the relevance of a selective interaction with buffers for the appearance of such structures in cells.[4] Another related example—not included in this paper—refers to the existence of Turing structures in the Selkov model of glycolysis [36]. While previous works [37] numerically supported the existence of a symmetry breaking instability of Turing type, those results were with unrealistic relations between the diffusion coefficients of very similar chemical species. However, the analysis of the reduced set of reaction diffusion equations shows that, without using a suitable tuned diffusion ratio, the possibility of finding Turing structures in cells by the Selkov mechanism was, at least, overestimated [35]. With all this in mind, it is clear that it becomes necessary to carefully assess the subtleties introduced by widespread used external agents or by endogenous buffers in the dynamical scenario.

In general, the behavior of a set of reaction-diffusion equations depends on the relative rates of diffusion and reaction. Quite often, we can think of a system as being in one of two extreme situations where the mathematical analysis is capable of being simplified. First, if diffusion is rapid compared with the reaction, the concentrations are effectively uniform throughout the medium, and the behavior is controlled solely by the reaction processes. This leads to a set of ordinary differential equations, which can be further reduced in number if reactions occur on several time scales using standard center manifold techniques. At the other limit, diffusion is slow compared with some (or maybe all) of the reactions. In this case, however, the simplification cannot be performed to such great extent as in the former situation, and thus it becomes important to fully understand the origin of the terms that we are likely to find under general reaction schemes [19]. The analysis presented in this paper shows how the reduced equations will reflect that the concentration of the different species reach local equilibrium values, and how the effective rate of the reaction will be regulated by the rate of supply of the reactants by the slow diffusive process. In this way we were able to understand the common chemical origin of both the rescaling of the self-diffusion terms, and the cross-diffusive terms that appear in the macroscopic equations. As shown in [19], more complex reaction schemes share with the ones analyzed in this paper the same type of terms in the phenomenological reduced equations, so the present analysis can also be extended to other cases, as the results obtained on the modified Schnackenberg model support.

ACKNOWLEDGMENTS

This work was supported by the University of Buenos Aires, CONICET (Argentina) and FOMEC. D.E.S. acknowledges useful discussions with M. G. Zimmermann.

APPENDIX

In this appendix, we give a brief description of the dynamics of the reactive lattice gas automaton (RLGA), where we show why it is not necessary to keep track of the particles' velocities if there is no exclusion principle. Consider a system of $\hat{S}$ chemical species $\mathcal{X}_1, \ldots, \mathcal{X}_{\hat{S}}$ that diffuse in solution and that undergo a set of chemical reactions of the type

$$\alpha_1^{(\prime)}\mathcal{X}_1+\cdots+\alpha_{\hat{S}}^{(\prime)}\mathcal{X}_{\hat{S}}\rightarrow\beta_1^{(\prime)}\mathcal{X}_1+\cdots+\beta_{\hat{S}}^{(\prime)}\mathcal{X}_{\hat{S}}, \quad \text{(A1)}$$

[4]We have also found analytically the—enlarged—Turing space of the modified Schnackenberg reaction diffusion equations. If the buffer concentration is large enough it is in principle possible to observe Turing structures with nearly equal diffusion coefficients. See [35].

where the ℓth reaction ($\ell=1,\ldots,R$) is characterized by both, the set of stoichiometric indices $\alpha_s^{(\ell)}$, $\beta_s^{(\ell)}$ ($s=1,\ldots,\hat{S}$) and the reaction rate constant k_ℓ. The aim is to construct an approximate dynamics for both the elastic and reactive collision processes that occur in the real system. In the RLGA model, the system evolves at discrete time steps of size τ on a d-dimensional regular lattice with lattice spacing λ, which for simplicity is taken to be a square lattice in two space dimensions (or a cube in three dimensions). Also for simplicity, we will only discuss the case of periodic boundary conditions (in which case all lattice sites are treated similarly, after an identification of the sites at the borders). In this Appendix we will take the particles' velocities into account, as it is done in RLGA that use the exclusion principle. We will then show why it is not necessary to keep track of these velocities, if there is no exclusion principle, as in our case. We will assume that each particle can have $\xi+1$ different velocities, where ξ is the number of nearest (different) nodes that each lattice site has ($\xi=2$ in one dimension and $\xi=4$ in two). During a time step τ, each particle can move to any of its nearest lattice sites, depending on its velocity, or stay, if it has velocity zero. Thus, the velocities $\vec{v}_i$ with $1\leqslant i\leqslant\xi$ are vectors of size λ/τ that connect neighboring lattice sites, and $\vec{v}_0=0$. A particular state of the RLGA is then characterized by $\hat{S}$ sets of non-negative integer variables, $f_s(\vec{r},\vec{v}_i,t)$, $s=1,\ldots,\hat{S}$, $0\leqslant i\leqslant\xi$, defined at each lattice site $\vec{r}$ and each time t. Each $f_s(\vec{r},\vec{v}_i,t)$ represents the number of particles of species $\mathcal{X}_s$ with velocity $\vec{v}_i$, at site $\vec{r}$ and time t. As mentioned before, the time step is divided in a diffusion (transport) time step (that changes all the distributions f_s from t to $t+\tau/2$) and a reactive time step (that changes the distributions from $t+\tau/2$ to $t+\tau$). Therefore, the system evolves through the successive application of the transport and reaction operators. One may visualize the dynamics of the entire system as a stack of $\hat{S}$ lattices (one for each species) with identical labeling of the nodes and of the particles' velocities. The transport operator is designed to model the elastic collisions of the particles with solvent molecules. The way in which this process is modeled by RLGA makes sense on a time scale of the order of the velocity relaxation time, and on a length scale that is larger than the mean free path of the particle [25]. Namely, it is assumed that several collisions take place during a time step, so that the final and initial velocities are not correlated. Thus, during the (diffusion) time step, each particle of species $\mathcal{X}_s$ can change its velocity to any velocity $\vec{v}_i$, $1\leqslant i\leqslant\xi$ with probability p_s and to velocity $\vec{v}_0=0$ with probability $1-\xi p_s$. Given that our lattice gas does not use the exclusion principle, the velocity can be any, no matter what velocities the other particles at the node have. After that, the particle is moved to the corresponding neighboring site, depending on the velocity it has ''picked.'' This is equivalent to make each particle perform a random walk, regardless of the last velocity it had. Namely, to choose its new location (among the current location and the nearest neighboring ones), regardless of the velocity it has. After the new location is chosen, the velocity can be set equal to the one that corresponds to the movement that the particle has performed. This can be written as

$$f_s(\vec{r},\vec{v}_i,t+\tau/2)=\mathcal{N}_s(\vec{r}-\vec{v}_i\tau,t-\tau)\times\sum_{j=1}^{\infty}\zeta_j^{(i)}\mathcal{H}(\mathcal{N}_s(\vec{r}-\vec{v}_i\tau,t-\tau)-\mu), \tag{A2}$$

where $\mathcal{N}_s(\vec{r},t)=\Sigma_i f_s(\vec{r},\vec{v}_i,t+\tau/2)$ is the total number of particles at point $\vec{r}$ and time t, the $\zeta_j^{(i)}$'s are random variables that can be equal to 1, with probability p_s, and equal to 0, with probability $1-p_s$ (with p_s satisfying $1-\xi p_s>0$), and $\mathcal{H}$ is the Heaviside function defined by $\mathcal{H}(y)=1$ if $y\geqslant 0$, and $\mathcal{H}(y)=0$ otherwise. Each random variable $\zeta_j^{(i)}$ is the ith component of a (random) $(\xi+1)$-uple in the set $\{(0,\ldots,0),(1,0,\ldots,0),(0,1,\ldots,0),\ldots(0,\ldots,1)\}$, where the probability of $(0,\ldots,0)$ is $1-\xi p_s$ and the probability of any other element in the set is p_s. At each diffusion time step we associate, according to the probability distribution, one element of this set to every particle in the lattice in order to decide if it is going to be moved and in which direction it will be moved. We see from Eq. (A2) that $f_s(\vec{r},\vec{v}_i,t+\tau/2)$ only depends on the total number of particles $\mathcal{N}_s$ at the previous time t (and the set of random variables $\zeta_j^{(i)}$), but not on the individual values of the distributions, $f_s(\vec{r}',\vec{v}_i,t)$, at the neighboring sites $\vec{r}'$. From Eq. (A2) we also conclude that the total number of particles at time $t+\tau/2$, $\mathcal{N}_s(\vec{r},t+\tau/2)$, only depends on the total number of particles that reside at neighboring sites at the previous time t.

The dynamics on the lattices that we associate to each species s is coupled by the chemical reaction. The reaction operation is local in space, i.e., it involves only one node on the stack of $\hat{S}$ lattices. The reaction operator $\mathcal{R}$ allows each reaction r to occur with a certain probability (associated to k_r) which is independent of the particles velocities, and, for those that do occur, it subtracts or adds the appropriate number of particles as dictated by Eq. (A1). Thus, the reaction operator only affects the total number of particles at each node in the following way:

$$\mathcal{R}\mathcal{N}_s(\vec{r},t)=\mathcal{N}_s(\vec{r},t)+\sum_{\ell=1}^{R}(\beta_s^{\ell}-\alpha_s^{\ell})\,\eta_{x,\ell}, \tag{A3}$$

where $\eta_{x,\ell}$ is a random boolean variable. If $\eta_{x,\ell}=1$, then the ℓth reaction takes place at the lattice site $\vec{r}$. The link between the probability distribution of the random boolean variable and the reaction rules that give the proper continuum limit, is achieved by choosing a function that depends on the occupation numbers (see [29] for a complete discussion on this topic).

From this discussion we immediately conclude that it is sufficient to work with the total number of particles $\mathcal{N}_s$ at each node and time, i.e., it is not necessary to keep track of

the particles' velocities, as mentioned in Sec. III. Some other points are worth mentioning too. First, that lattice gases for reaction-diffusion systems do not suffer from the same sort of drawback that other kind of lattice gases (in particular, those used to model the Navier-Stokes equation) do. Namely, for RLGA there are no spurious conservation laws associated with a square lattice geometry. Second, we want to emphasize that it was unnecessary to choose a particular reaction rule to derive the analytical results in Secs. III and IV. This is so, because any particular choice of the reaction operator should project, in a similar way, the mean concentration values onto the local equilibrium values of each species.

[1] G. Nicolis and I. Prigogine, *Self-Organization in Nonequilibrium Systems* (Wiley, New York, 1977).

[2] A.S. Mikhailov, *Foundations of Synergetics I* (Springer-Verlag, Berlín, 1991).

[3] A.M. Turing, Philos. Trans. R. Soc. London, Ser. B **237**, 37 (1952).

[4] J.D. Murray, *Mathematical Biology* (Springer, New York, 1989), Chap. 12.

[5] F. Reif, *Fundamentals of Statistical and Thermal Physics* (McGraw-Hill, New York, 1965).

[6] M.C. Cross and P.C. Hohenberg, Rev. Mod. Phys. **65**, 851 (1993).

[7] S.P. Dawson, M.V. D'Angelo, and J.E. Pearson, Phys. Lett. B **B265**, 346 (2000).

[8] S. Kondo and R. Asai, Nature (London) **376**, 765 (1995).

[9] S. Sawai, Y. Maeda, and Y. Sawada, Phys. Rev. Lett. **85**, 2212 (2000).

[10] V. Castets, E. Dulos, J. Boissonade, and P. De Kepper, Phys. Rev. Lett. **64**, 2953 (1990).

[11] Q. Ouyang and H. Swinney, Nature (London) **352**, 610 (1991).

[12] I. Lengyel and I. Epstein, Science **251**, 650 (1991).

[13] J. Wagner and J. Keizer, Biophys. J. **67**, 447 (1994).

[14] N.L. Allbritton, T. Meyer, and L. Stryer, Science **258**, 1812 (1992).

[15] W.M. Roberts, J. Neurosci. **14**, 3246 (1994).

[16] G.D. Smith, Biophys. J. **71**, 3064 (1996); G.D. Smith, J. Wagner, and J. Keizer, *ibid.* **70**, 2527 (1996).

[17] M. Naraghi and E. Neher, J. Neurosci. **17**, 6961 (1997).

[18] M.J. Berridge, M.D. Bootman, and P. Lipp, Nature (London) **395**, 645 (1998).

[19] D.E. Strier and S.P. Dawson, J. Chem. Phys. **112**, 825 (2000).

[20] E.J. Hinch, *Perturbation Methods* (Cambridge University Press, Mexico City, 1992), p. 116.

[21] This equation has also been used to model the absortion of a diffusing substance by a solid body, see, e.g., M. Sahimi, Rev. Mod. Phys. **65**, 1393 (1993).

[22] J.E. Pearson and W. Bruno, Chaos **2**, 513 (1992).

[23] S.P. Dawson, A. Lawniczak, and R. Kapral, J. Chem. Phys. **100**, 5211 (1994).

[24] J. Schnackenberg, J. Theor. Biol. **81**, 389 (1979).

[25] J.P. Boon, D. Dab, R. Kapral, and A. Lawniczak, Phys. Rep. **273**, 2 (1996).

[26] In the case in which there are n extra species that react among themselves and with $\mathcal{A}$ at a slow rate, but do not react with the buffers (B) (i.e., are not involved in the fast reaction), then the reduction yields $n+1$ evolution equations plus the algebraic relations $B=k_dB_T/(k_d+A)$ and (8). One of the evolution equations is not of reaction-diffusion type (the equation for A).

[27] S. Chen, S.P. Dawson, G.D. Doolen, D.R. Janecky, and A. Lawniczak, Comput. Chem. Eng. **19**, 10 (1995).

[28] B. Chopard, M. Droz, S. Cornell, and L. Frachebourg, in *Cellular Automata: Prospects in Astrophysical Applications*, edited by J.M. Perdang and A. Lejeune (World Scientific, Singapore, 1993).

[29] T. Karapiperis and B. Blankleider, Physica D **78**, 30 (1994).

[30] D.H. Zanette, Phys. Rev. A **46**, 7573 (1992).

[31] G. Macnamara and G. Zanetti, Phys. Rev. Lett. **61**, 2332 (1988); S.P. Dawson, S. Chen, and G.D. Doolen, J. Chem. Phys. **98**, 1514 (1993).

[32] N.G. van Kampen, *Stochastic Processes in Physics and Chemistry* (North-Holland, Amsterdam, 1981).

[33] B.C. Goodwin, J.D. Murray, and D. Baldwin, in *Proceedings of the 6th International Symposium on Acetabularia, Pisa, 1984*, edited by S. Bonotto, F. Cinelli, and R. Billiau (Belgian Nuclear Center, C.E.N.-S.C.K., Mol, Belgium, 1985).

[34] J.J. Falke *et al.*, Q. Rev. Biophys. **27**, 219 (1994).

[35] D. E. Strier and S. P. Dawson (to be published).

[36] E.E. Selkov, Eur. J. Biochem. **4**, 79 (1968).

[37] B. Hasslacher, R. Kapral, and A. Lawniczak, Chaos **3**, 7 (1993).

[38] R. Kapral, A. Lawniczak, and P. Masiar, J. Chem. Phys. **96**, 2762 (1992).